T Cells Specific for a Mycobacterial Glycolipid Expand after Intravenous Bacillus Calmette-Guérin Vaccination

Layton, Erik D; Barman, Soumik; Wilburn, Damien B; Yu, Krystle K Q; Smith, Malisa T; Altman, John D; Scriba, Thomas J; Tahiri, Nabil; Minnaard, Adriaan J; Roederer, Mario

Published in:
Journal of Immunology

DOI:
10.4049/jimmunol.2001065

Publication date:
2021

The Journal of Immunology

T Cells Specific for a Mycobacterial Glycolipid Expand after Intravenous Bacillus Calmette–Guérin Vaccination

Erik D. Layton, Soumik Barman, Damien B. Wilburn, Krystle K. Q. Yu, Malisa T. Smith, John D. Altman, Thomas J. Scriba, Nabil Tahiri, Adriaan J. Minnaard, Mario Roederer, Robert A. Seder, Patricia A. Darrah and Chetan Seshadri

J Immunol 2021; 206:1240-1250; Prepublished online 3 February 2021;
doi: 10.4049/jimmunol.2001065
http://www.jimmunol.org/content/206/6/1240

The Journal of Immunology is published twice each month by
The American Association of Immunologists, Inc.,
1451 Rockville Pike, Suite 650, Rockville, MD 20852

Print ISSN: 0022-1767 Online ISSN: 1550-6606.

T Cells Specific for a Mycobacterial Glycolipid Expand after Intravenous Bacillus Calmette–Guérin Vaccination

Erik D. Layton,* Soumik Barman,*,[1] Damien B. Wilburn,[†] Krystle K. Q. Yu,* Malisa T. Smith,* John D. Altman,[‡] Thomas J. Scriba,[§] Nabil Tahiri,[¶] Adriaan J. Minnaard,[¶] Mario Roederer,[‖] Robert A. Seder,[‖] Patricia A. Darrah,[‖] and Chetan Seshadri*,[#]

Intradermal vaccination with *Mycobacterium bovis* bacillus Calmette–Guérin (BCG) protects infants from disseminated tuberculosis, and i.v. BCG protects nonhuman primates (NHP) against pulmonary and extrapulmonary tuberculosis. In humans and NHP, protection is thought to be mediated by T cells, which typically recognize bacterial peptide Ags bound to MHC proteins. However, during vertebrate evolution, T cells acquired the capacity to recognize lipid Ags bound to CD1a, CD1b, and CD1c proteins expressed on APCs. It is unknown whether BCG induces T cell immunity to mycobacterial lipids and whether CD1-restricted T cells are resident in the lung. In this study, we developed and validated *Macaca mulatta* (*Mamu*) CD1b and CD1c tetramers to probe ex vivo phenotypes and functions of T cells specific for glucose monomycolate (GMM), an immunodominant mycobacterial lipid Ag. We discovered that CD1b and CD1c present GMM to T cells in both humans and NHP. We show that GMM-specific T cells are expanded in rhesus macaque blood 4 wk after i.v. BCG, which has been shown to protect NHP with near-sterilizing efficacy upon *M. tuberculosis* challenge. After vaccination, these T cells are detected at high frequency within bronchoalveolar fluid and express CD69 and CD103, markers associated with resident memory T cells. Thus, our data expand the repertoire of T cells known to be induced by whole cell mycobacterial vaccines, such as BCG, and show that lipid Ag-specific T cells are resident in the lungs, where they may contribute to protective immunity. ***The Journal of Immunology*****, 2021, 206: 1240–1250.**

Mycobacterium bovis bacillus Calmette–Guérin (BCG) is the oldest vaccine still in clinical use today, with over 3 billion doses administered since 1921 (1). In most countries, infants undergo intradermal vaccination with BCG at birth, which protects them from disseminated tuberculosis and death in early childhood (2). BCG provides variable efficacy against tuberculosis disease when provided later in life (3). The reasons for this discrepancy are not fully understood but may relate to qualitative differences in the adaptive immune response to BCG (1).

Studies in mice and nonhuman primates (NHP) show that T cells are critical for the protective efficacy of BCG. T cell–deficient mice fail to control *M. tuberculosis* to the same extent as wild-type mice after BCG (4). CD8 T cell depletion in NHP abrogates the protective effect of BCG (5). More recently, i.v. BCG was shown to provide superior protection to *M. tuberculosis* challenge in rhesus macaques when compared with the standard intradermal route (6, 7). Higher levels of Ag-specific T cells in the lung and bronchoalveolar lavage (BAL) fluid were induced by i.v. BCG, suggesting that they may be directly responsible for improved protection (6).

Canonically, T cells are activated by foreign peptide Ags presented by autologous MHC molecules (8). However, during vertebrate evolution, T cells have also acquired the capacity to recognize bacterial lipid Ags via the CD1 lipid Ag presentation pathway (9). Humans express four CD1 Ag-presenting molecules (CD1a, CD1b, CD1c, and CD1d), which vary in the configuration of their binding grooves, patterns of cellular expression, and subcellular trafficking (10). The first structurally defined lipid Ag was mycolic acid, which is composed of long (C_{80}) alkyl chains, is a ubiquitous component of the mycobacterial cell wall, and is presented by CD1b to T cells (11). Follow-up studies identified the structurally related Ags glucose monomycolate (GMM) and glycerol monomycolate (12, 13). Several other mycobacterial lipid Ags have been discovered as T cell Ags, whose recognition is mediated by CD1a, CD1b, or CD1c (group 1) in humans (10). Current evidence suggests that these lipid-specific T cells are expanded in clinical settings of mycobacterial exposure or infection

*Department of Medicine, University of Washington School of Medicine, Seattle, WA 98109; [†]Department of Genome Sciences, University of Washington School of Medicine, Seattle, WA 98195; [‡]National Institutes of Health Tetramer Core Facility, Emory University, Atlanta, GA 30329; [§]South African Tuberculosis Vaccine Initiative, Institute of Infectious Disease and Molecular Medicine, University of Cape Town, Cape Town 9747, South Africa; [¶]Stratingh Institute for Chemistry, University of Groningen 7925, Groningen, the Netherlands; [‖]Vaccine Research Center, National Institutes of Health, Bethesda, MD 20892; and [#]Tuberculosis Research and Training Center, University of Washington, Seattle, WA 98109

[1]Current address: Precision Vaccines Program, Division of Infectious Diseases, Boston Children's Hospital and Harvard Medical School, Boston, MA.

ORCIDs: 0000-0001-6409-290X (E.D.L.); 0000-0002-1255-9982 (D.B.W.); 0000-0001-8738-1579 (K.K.Q.Y.); 0000-0001-9733-2359 (J.D.A.); 0000-0002-0641-1359 (T.J.S.); 0000-0002-5966-1300 (A.J.M.); 0000-0002-0035-2802 (P.A.D.); 0000-0003-2783-7540 (C.S.).

Received for publication September 22, 2020. Accepted for publication January 1, 2021.

This work was supported by grants from the Bill and Melinda Gates Foundation (OPP1190451 to C.S.) and the National Institutes of Health (R01-AI125189 and R01-AI146072 to C.S.).

Address correspondence and reprint requests to Dr. Chetan Seshadri, University of Washington School of Medicine, 750 Republican Street, Suite E663, Seattle, WA 98109. E-mail address: seshadri@u.washington.edu

The online version of this article contains supplemental material.

Abbreviations used in this article: Ac_2SGL, diacylated sulfoglycolipid; BAL, bronchoalveolar lavage; BCG, bacillus Calmette–Guérin; EV, empty vector; α-GalCer, α-galactosylceramide; GMM, glucose monomycolate; hCD1Tg, humanized CD1 transgenic; iNKT, invariant NKT; MAIT, mucosal-associated invariant T; NHP, nonhuman primate; NIH, National Institutes of Health; 5-OP-RU, 5-(2-oxopropylideneamino)-6-D-ribitylaminouracil; PM, phosphomycoketide; rhIL-2, recombinant human IL-2; T_{EM}, effector memory T; T_{RM}, tissue-resident memory T; UMAP, Uniform Manifold Approximation and Projection.

(13–16). Lipid-loaded CD1 tetramers have facilitated further ex vivo studies of the phenotypes of CD1-restricted T cells in humans (17–21). T cell recognition of GMM is exquisitely sensitive to the position of the glucose headgroup but relatively independent of lipid chain length, allowing both short-chain (C_{32}) and C_{80}-GMM to be used in tetramers (12, 17, 22). Other studies have revealed that germline-encoded residues within TRAV1-2 are required for recognition of GMM and that TRBV4-1 may bias T cells toward recognition of CD1b and CD1c (17, 23–25). Because CD1 genes exhibit very few polymorphisms in humans, CD1 tetramers can be used without prior knowledge of genotype, enabling population-based studies (15, 26).

Further studies elucidating the contribution of CD1a-, CD1b-, and CD1c-restricted T cells to protective immunity during *M. tuberculosis* infection have been hampered by the lack of a suitable animal model. Mice have only one ortholog of human CD1d, so this model has provided a narrow window into the role of CD1d-restricted invariant NKT (iNKT) cells in tuberculosis (27, 28). Genomic studies suggest that CD1a, CD1b, and CD1c genes were deleted from Rodentia or a common ancestor (29). Humanized CD1 transgenic (hCD1Tg) mice express CD1a, CD1b, and CD1c in a pattern similar to that seen in humans and support the development of group 1 CD1-restricted T cells (30). Infection of hCD1Tg mice with BCG induces mycolic acid–specific T cells, which home to pulmonary granulomas and mediate partial protection after *M. tuberculosis* challenge in a CD1-restricted manner (31). CD1b was shown to be expressed in human granulomas as well as conserved TCR sequences expressed by CD1b-restricted T cells (32, 33). Whether BCG induces T cell responses to mycobacterial lipids in humans and NHP is currently not known.

Evolutionary genetic analysis suggests that mice are the exception among mammals, most of which have expanded CD1 gene families similar to humans (34). Specifically, a five-gene CD1 locus is highly conserved between humans and NHP, which stands in stark contrast to genes encoded within the MHC (35). Several studies have investigated the phenotypes and functions of iNKT cells in NHP (35–37). However, there have been only a few attempts to explore CD1-restricted T cells. One effort using a human lymphoblastoid cell line (T2) stably transfected with *Macaca mulatta* (*Mamu)* CD1b was able to activate a Jurkat cell line transfected with a GMM-specific human TCR in the presence of GMM (38). Another study explored the restriction of T cells induced by repeated vaccination with BCG and a liposomal formulation of GMM. Notably, GMM-reactive T cells were detected in the blood, but these were restricted by *Mamu* CD1c rather than *Mamu* CD1b (39). These limited and conflicting data suggest that T cells specific for mycobacterial glycolipids may be induced by vaccination, but their restricting element, phenotypes, and tissue distribution have not been determined.

We generated *Mamu* CD1b and *Mamu* CD1c tetramers and validated their ability to detect GMM-specific T cells by sorting them from the blood of BCG-vaccinated animals and performing in vitro expansion and functional assays. We find that the response to GMM is restricted by CD1b and CD1c in NHP and, surprisingly, in humans as well. We incorporated CD1c-GMM tetramers into a multiparameter flow cytometry panel and show that GMM-specific T cells are expanded in the blood of NHP 4 wk after i.v. BCG with a predominant effector memory T (T_{EM}) phenotype. These cells are also detectable in the lung as tissue-resident memory T (T_{RM}) cells 4 wk after vaccination. These data establish the NHP as a natural model to study CD1-restricted T cells, which are resident in the lung and may contribute to protective immunity induced by whole cell mycobacterial vaccines.

Materials and Methods

Evolutionary genetic analysis of group 1 CD1 genes

CD1a, CD1b, and CD1c sequences were collected for 11 primate species with sequenced genomes (human, chimpanzee, bonobo, gorilla, gibbon, orangutan, rhesus macaque, crab-eating macaque, green monkey, olive baboon, and marmoset) using a custom bioinformatics pipeline adapted from Young and Trask (40). Briefly, the Basic Local Alignment Search Tool (tblastn) was used with human CD1a, CD1b, and CD1c protein sequences as queries to identify potentially homologous regions in each primate genome. Putative exons were defined based on a low e-value ($<1 \times 10^{-8}$), contiguity in sequence orientation, and proximity within 20 kb. These putative loci were extracted and analyzed using exonerate in protein-to-genome mode with human group 1 CD1 sequences as queries to identify putative open reading frames. For each paralog, sequences were aligned using Clustal Ω (41), and tests of positive selection were performed using the codeml application in PAML (v4.8) with the primate species tree (42). Gene duplications of CD1A in olive baboon (two copies) and marmoset (three copies) were included as polytomies on the species tree. The nested models of neutral evolution (M8a) and one allowing for positive selection (M8) were compared by likelihood-ratio test (43), and if significant, sites with Bayes-empirical Bayes-posterior probabilities ≥0.8 were considered under positive selection. Positively selected sites were modeled onto available crystal structures (Protein Data Bank numbers 5J1A, 5L2J, and 3OV6 for CD1a, -b, and -c, respectively) using PyMOL v2.4.

Preparation of lipid-loaded CD1 tetramers

C_{32}-GMM isolated from *Rhodococcus equi*, synthetic phosphomycoketide (PM), and diacylated sulfoglycolipid (Ac_2SGL) were generously provided by the laboratory of D. B. Moody (20, 44, 45). Synthetic C_{80}-GMM was prepared as we recently described (45). Stock GMM, PM, or Ac_2SGL was solvated in chloroform/methanol (2:1, v/v) at a concentration of 1 mg/ml. *Mamu* and *Homo sapiens* CD1b and CD1c biotinylated monomers were provided by the National Institutes of Health (NIH) Tetramer Core Facility (Emory University, Atlanta, GA). GMM-loaded CD1b tetramers were generated as previously described with the following modifications: C_{32}-GMM was used at a 40-fold excess, and lipid loading was performed overnight at 37˚C (15). GMM-loaded CD1c tetramers were generated as follows: a 100-fold excess of C_{32}-GMM was aliquoted into a single-use glass vial and evaporated under a nitrogen stream to remove the solvent. One hundred microliters of PBS was added, and the vial was sonicated at 37˚C for 15 min and then moved to the 37˚C water bath. Following the addition of CD1c monomer, the solution was incubated at 37˚C overnight. On the following day, streptavidin (Life Technologies, Carlsbad, CA; BioLegend, San Diego, CA; BD Biosciences, San Jose, CA) was added to tetramerize the CD1c monomers. The tetramer was filtered through a Spin-X column (Sigma-Aldrich, St. Louis, MO) to remove large aggregates and stored at 4˚C until use. CD1b and CD1c mock-loaded tetramers were generated in an analogous manner but without the addition of lipid Ag. MR1–5-(2-oxopropylideneamino)-6-D-ribitylaminouracil (5-OP-RU) and CD1d–α-galactosylceramide (α-GalCer) tetramers were provided by the NIH Tetramer Core Facility.

Generation of monocyte-derived dendritic cells

PBMCs were isolated from human (Bloodworks, Seattle, WA) or NHP whole blood (Washington National Primate Research Center, Seattle, WA) by density centrifugation with Ficoll-Paque PLUS media (Cytiva, Marlborough, MA) and plated in tissue culture dishes at a density of 10 million cells/ml in R10 media (RPMI 1640 [Life Technologies] with 10% FBS [Hyclone Laboratories, Logan, UT]), supplemented with recombinant human GM-CSF (final concentration of 100 ng/ml) (PeproTech, Cranbury, NJ) and incubated at 37˚C for 3 h. After incubation, residual nonadherent cells were removed by washing gently with R10. R10 supplemented with rhGM-CSF (final 100 ng/ml) and rhIL-4 (final 20 ng/ml) (PeproTech) was added to the adherent fraction, and the cells were then incubated at 37˚C for 3 d (46). Following the incubation period, adherent monocyte-derived dendritic cells were harvested and cryopreserved in liquid nitrogen. Cells were screened by flow cytometry for CD1 expression by staining with the following anti-human CD1 Abs: anti-CD1a PE (clone HI149), anti-CD1b FITC (clone SN13), anti-CD1c allophycocyanin (clone L161) (BioLegend), and anti-CD1d PE (clone 42.1) (BD Biosciences).

Generation of human and NHP T cell lines

Cryopreserved human PBMC were thawed and rested overnight and then mixed with γ-irradiated (5000 rad) allogeneic monocyte-derived dendritic

cells at a ratio of 5:1 and incubated in T cell media (R10 supplemented with 100 U/ml penicillin, 100 mg/ml streptomycin, 55 mM 2-ME, 0.3× essential amino acids, 60 mM nonessential amino acids, 11 mM HEPES, and 800 mM L-glutamine [Life Technologies]) with 1 μg/ml of C_{32}-GMM and 50 U/ml recombinant human IL-2 (rhIL-2; Prometheus Laboratories through University of Washington Medical Center clinical pharmacy) for 12–14 d. T cell lines were screened with *H. sapiens* CD1b-GMM or *H. sapiens* CD1c-GMM tetramer. To further purify GMM-specific T cells present within T cell lines, cells were stained with PE-conjugated tetramers in FACS buffer without additional additives. An anti-streptavidin PE Ab (clone 3A20.2) (BioLegend) was also included to enhance the fluorescence intensity of tetramer-specific cells (47). After Ab staining, the cells were resuspended in culture media and kept on ice until sorting. Tetramer-positive T cells were sorted at the University of Washington's Department of Immunology Flow Cytometry Core using an FACSAria II (BD Biosciences) cell sorter equipped with violet (407-nm), blue (488-nm), and red (641-nm) lasers.

Sorted T cells were expanded using a modified version of a previously published rapid expansion protocol (48). Briefly, T cells were mixed with 5 million γ-irradiated (8000 rad) lymphoblastoid cells (courtesy of D. Koelle, University of Washington) and 25 million γ-irradiated (3300 rad) PBMC provided by an anonymous blood donor to act as feeder cells in T25 tissue culture flasks (Costar, St. Louis, MO). Anti-CD3 (clone OKT3) was added at a final concentration of 30 ng/ml, and the mixture was incubated overnight at 37˚C. On the following day, rhIL-2 was added to a final concentration of 50 U/ml. On day 4, the cells were washed twice in T cell media to remove the anti-CD3 Ab and resuspended in fresh media supplemented with rhIL-2 at 50 U/ml. Half the media was replaced every 3 d or split into new T25 flasks as determined by cell confluency. After 13 d in culture, T cell lines were screened using *H. sapiens* CD1b-GMM or *H. sapiens* CD1c-GMM tetramer. T cell lines were cryopreserved until use.

To generate NHP T cell lines, cryopreserved PBMC were thawed and rested overnight and then mixed with γ-irradiated *Mamu* allogeneic monocyte-derived dendritic cells and C_{32}-GMM as described above. After 2 wk in culture, T cells were stained using *Mamu* CD1b-GMM or *Mamu* CD1c-GMM tetramer, and tetramer-positive T cells were sorted as above. Sorted T cells were expanded in vitro using the rapid expansion method detailed above, except that irradiated *Mamu* PBMC and splenocytes were used as feeder cells. Repeated rounds of expansion were achieved by using γ-irradiated human PBMC and lymphoblastoid cells in the presence of rhIL-2 and/or PHA (Remel, San Diego, CA).

Flow cytometry

PBMC or T cell lines were thawed in RPMI 1640 (Life Technologies) supplemented with 10% FBS (Atlas Biologicals, Fort Collins, CO), and viable cells were enumerated by trypan blue (MilliporeSigma, Burlington, MA) exclusion. The PBMC or T cell lines were plated at a final density of 1 million cells per well and then washed twice with 1× PBS (Life Technologies). The cells were then stained with Aqua LIVE/DEAD (Life Technologies) according to manufacturer's instructions and incubated for 15 min at room temperature. LIVE/DEAD staining and all following steps were performed in the dark. At the end of the incubation, cells were washed twice in PBS and blocked by incubating the cells with human serum (Valley Biomedical, Winchester, VA) and FACS buffer (PBS supplemented with 0.2% BSA [Sigma-Aldrich]) mixed 1:1 for 15 min at 4˚C. Anti-CCR7 Ab (BD Biosciences) was then prepared with 50 nM dasatinib (Cayman Chemical, Ann Arbor, MI), and the cells were incubated with the solution at 37˚C for 30 min (47). The wells were then washed with FACS buffer and resuspended in FACS buffer containing 50 nM dasatinib and lipid or mock-loaded CD1 tetramers for 60 min at room temperature. At the end of the incubation, the cells were washed twice in FACS buffer and then stained with Abs prepared in FACS buffer containing 1 mM ascorbic acid and 0.05% sodium azide (49). Markers included anti-CD3 BUV395 (clone UCHT1) (BD Biosciences), anti-CD3 PerCP Cy5.5 (clone SP34-2) (BD Biosciences), anti-CD4 allophycocyanin–H7 (clone L200) (BD Biosciences), anti-CD8 BV785 (clone RPA-T8) (BioLegend), anti–TRAV1-2 BV605 (clone 3C10), and anti–TRBV4-1 PE (clone ZOE) (Beckman Coulter, Brea, CA). The Ab mixture was centrifuged at 10,000 × *g* for 5 min to remove aggregates and then incubated with the cells for 30 min at 4˚C. The samples were washed in FACS buffer and then fixed in PBS containing 1% paraformaldehyde (Electron Microscopy Sciences, Hatfield, PA) for 15 min at 4˚C. After two final washes in PBS, the cells were resuspended in PBS containing 2 mM EDTA to prevent clumping and then stored at 4˚C until acquisition. Samples were acquired on a BD LSRFortessa (BD Biosciences) equipped with blue (488-nm), green (532-nm), red (628-nm), violet (405-nm), and UV (355-nm) lasers.

For results described in Figs. 4 and 5, the rhesus macaque PBMC and BAL samples were thawed in warm media consisting of R10 and 2 μl/ml Benzonase (MilliporeSigma) sterile-filtered and centrifuged at 250 × *g* for 10 min. The supernatant was decanted, and the viable cells were enumerated using Guava Viacount Reagent (MilliporeSigma) and acquired on a Guava easyCyte Benchtop Flow Cytometer (MilliporeSigma) according to manufacturer's instructions. The cells were centrifuged at 250 × *g* for 10 min and rested overnight at a density of 2 million cells/ml. On the following day, the cells were counted and plated at a density of 4 million cells per well in a 96-well U-bottom plate. The staining procedure was performed as above with the following reagents: *H. sapiens* CD1d–α-GalCer PE Tetramer, *Mamu* MR1–5-OP-RU BV421 Tetramer (NIH Tetramer Core Facility, Atlanta, GA), *Mamu* CD1c-GMM BV650 tetramer, *Mamu* CD1c-GMM PE-Cy7 tetramer, *Mamu* CD1c-mock PerCP Cy5.5 tetramer (custom), anti-CD3 BUV737 (clone SP34-2), anti-CD4 allophycocyanin–H7 (clone L200), anti-CD45RA PE-Cy5 (clone 5H9), anti-TCR γ/δ PE-Dazzle594 (clone B1), anti-CCR7 BUV395 (clone 150503) (BD Biosciences), anti-CD8α BV785 (clone RPA-T8), anti-CD14 allophycocyanin (clone M5E2), anti-CD69 BV711 (clone FN50), anti-TCR Vδ2 AF700 (clone B6), anti–HLA-DR BV570 (clone L243) (BioLegend), anti-CD19 allophycocyanin (clone CB19; Abcam, Cambridge, U.K.), anti-CD38 FITC (clone AT-1; STEMCELL Technologies, Vancouver, Canada), anti-CD103 Super Bright 600 (clone B-Ly-7; eBioscience, San Diego, CA), and LIVE/DEAD Fixable Aqua (Life Technologies). Samples from 10 animals were processed, and flow cytometry data were acquired in two batches in which PBMC and BAL samples were evenly distributed. However, the BAL sample from one rhesus macaque was not used because of sample quality.

IFN-γ ELISPOT

To test the functional response of human T cell lines, Multiscreen-IP Filter Plates (MilliporeSigma) were first coated with an anti–IFN-γ Ab (clone 1-D1K) (Mabtech, Nacka Strand, Sweden) diluted 1:400 in PBS and incubated overnight at 4˚C. On the following day, 4000 T cells were plated with 50,000 human myelogenous leukemia cells (K562) stably transfected with human CD1a, CD1b, CD1c, CD1d, or with a mock vector (empty vector [EV]) (50). Lipid Ags were stored in chloroform:methanol (2:1, v/v) prior to drying using gaseous nitrogen. The lipids were sonicated into media and added to the cultures at a final concentration of 1 μg/ml. The cultures were incubated at 37˚C for ∼16 h and washed twice with sterile water to lyse the cells, and the plates were incubated with the detection Ab 7-B6-1 (Mabtech) diluted to 1 μg/ml in PBS/0.5% FBS and incubated for 2 h at room temperature. The cells were then washed five times with PBS. One hundred microliters of ExtrAvidin–Alkaline Phosphatase (Sigma-Aldrich) diluted 1:1000 in PBS/0.5% FBS was then added, and the plates were incubated for 1 h at room temperature. The samples were washed five times and incubated with BCIP/NBT substrate (Sigma-Aldrich) prepared according to manufacturer's instructions for 15 min in the dark at room temperature to develop the membrane. IFN-γ spots were measured using an ImmunoSpot S6 Core Analyzer (Cellular Technology, Cleveland, OH).

Detection of IFN-γ produced by *Mamu* T cells was performed similarly but with the following modifications: a MultiScreen PVDF Plate (MilliporeSigma) was wetted using 15 μl of 35% ethanol for no longer than 1 min. The plate was then washed with sterile water five times before coating the plate with 100 μl of PBS containing 15 μg/ml of anti-human IFN-γ Ab (clone MT126L) (Mabtech) and incubating overnight at 4˚C.

Animals

Derivation of macaque T cell lines began with PBMC isolation from a female Chinese rhesus macaque 12 wk after intradermal vaccination with BCG. Data presented in Figs. 4 and 5 derived from 10 Indian-origin rhesus macaques who underwent i.v. vaccination with 3×10^8 CFU/ml of Danish strain 1331 BCG as part of a larger study that was recently published (6). Cryopreserved PBMCs derived from blood collected at baseline or 4 wk postvaccination as well as BAL collected 4 wk postvaccination were used for the experiments described in this study.

All experimentation complied with ethical regulations established by the Animal Care and Use Committee of the Vaccine Research Center, National Institute of Allergy and Infectious Disease, NIH, and Environmental Health & Services at the University of Washington. Macaques were housed and cared for in accordance with local, state, federal, and institute policies in facilities accredited by the American Association for Accreditation of Laboratory Animal Care, under standards established in the Animal Welfare Act and the Guide for the Care and Use of Laboratory Animals. Macaques were monitored for physical health, food consumption, body weight, temperature, complete blood counts, and serum chemistries.

Clinical cohort

Derivation of human T cell lines began with cryopreserved PBMC donated by a South African adolescent who was enrolled into a study that aimed to determine the incidence and prevalence of tuberculosis infection and disease (51). Twelve- to eighteen-year-old adolescents were enrolled at high schools in the Worcester region of the Western Cape of South Africa. Subjects were screened for the presence of latent tuberculosis by a tuberculin skin test and IFN-γ release assay QuantiFERON-TB Gold In-Tube (QIAGEN, Hilden, Germany) at study entry. PBMC were isolated from freshly collected heparinized blood via density centrifugation and cryopreserved. For this study, we chose a single donor with latent tuberculosis from whom sufficient PBMC were archived for the proposed experiments.

Ethics

Clinical study protocols were approved by the institutional review boards of the University of Cape Town and the University of Washington. Written informed consent was obtained from parents and/or legal guardians of the adolescents who participated. In addition, written informed assent was obtained from the adolescents.

Data analysis and statistics

Initial compensation, gating, and quality assessment of flow cytometry data were performed using FlowJo version 9.9.6 (FlowJo; TreeStar, Ashland, OR). Boolean gating and subsequent analysis was performed using the OpenCyto framework in the R programming environment (52, 53). Cell frequencies were compared using Wilcoxon signed-rank tests and results are reported as unadjusted p values. Two pre-BCG PBMC samples were excluded during analysis because of low viability and low CD3 cell counts.

Uniform Manifold Approximation and Projection (UMAP) was performed using the uwot package in R (L. McInnes, J. Healy, and J. Melville, manuscript posted on arXiv, DOI: 1802.03426) with the following parameters: spread = 10 and min_dist = 0.15 for the *Mamu* CD1c-GMM tetramer data; spread = 16 and min_dist = 0.2 for the *H. sapiens* CD1d–α-Galcer tetramer data; and spread = 9 and min_dist = 0.02 for the *Mamu* MR1–5-OP-RU tetramer data. For the analysis of data generated using *Mamu* MR1 tetramer, cells were sampled evenly from each batch, tissue, and animal. However, for data generated using *Mamu*-CD1c and *H. sapiens*–CD1d tetramers, animals were unevenly sampled because of low cell counts. The following markers were used in the UMAP analysis: CD45RA, CD69, CD103, CCR7, CD38, γδ, CD4, δ2, CD8, HLA-DR, CD3, *Mamu* CD1c-GMM PE-Cy7, *Mamu* CD1c-GMM BV650, *H. sapiens* CD1d–α-GalCer, and *Mamu* MR1–5-OP-RU. Fluorescence intensities of each markers were scaled within each batch prior to running UMAP. The raw data and analysis code used to generate the figures in this manuscript are available upon reasonable request.

Results

Evolutionary genetics of group 1 CD1 genes among primates

We recently showed that a five-gene CD1 locus is present among all primate clades and that CD1d shows evidence of purifying selection during primate evolution. This allowed us to use *H. sapiens* CD1d tetramer loaded with α-GalCer to study the molecular mechanisms of Ag recognition by iNKT cells in rhesus macaques (35). To further delineate the evolutionary history of simian *CD1A*, *CD1B*, and *CD1C* genes, CD1 homolog sequences were mined from 11 primate genomes that include great apes, Old World monkey, and New World monkeys, spanning ∼45 million years of evolutionary time. In contrast to the very high conservation of *CD1D*, tests of molecular evolution across primates found significant signatures of diversifying (positive) selection in *CD1A*, *CD1B*, and *CD1C* (Table I). The signal is most robust in *CD1A*, which was also found to have experienced gene duplication independently in both olive baboon and marmosets (35). When the sites under positive selection were visualized on *H. sapiens*–derived crystal structures, most sites were localized within the lipid Ag binding pocket (Fig. 1A) (54–56). These data reveal that *CD1A*, *CD1B*, and *CD1C* have undergone diversifying selection during primate evolution, possibly leading to differences in the ability to bind and present lipid Ags to T cells.

GMM is presented by CD1b to T cells in macaques

We used the sequences for CD1b and CD1c obtained from cynomolgus macaques (*M. fascicularis*) and rhesus macaques (*M. mulatta*) to generate species-specific CD1b and CD1c tetramers (Supplemental Fig. 1). We used an established loading protocol to generate *Mamu* CD1b loaded with C_{32}-GMM and tested its ability to stain a human GMM-specific T cell line (G02) (17). We found that *Mamu* CD1b-GMM successfully stained human T cells compared with mock-loaded control tetramer but at a lower mean fluorescence intensity compared with *H. sapiens* CD1b-GMM (Fig. 1B). The human GMM-specific T cell repertoire consists of high-avidity T cells expressing TRAV1-2 or low-avidity T cells expressing TRBV4-1 (57, 58). We considered the possibility that *Mamu* CD1b-GMM might be missing some of these specific subpopulations. However, we found that *Mamu* CD1b-GMM detected similar proportions of T cells expressing TRAV1-2 or TRBV4-1 as *H. sapiens* CD1b-GMM (Fig. 1C). *Mamu* CD1b-GMM tetramer stained 0.1% of T cells in PBMC of a BCG-vaccinated rhesus macaque compared with a mock-loaded control tetramer (Fig. 1D). These T cells were sorted and successfully expanded ∼100-fold into a T cell line (bG52R). Because human PBMC were used as feeder cells, we verified the species origin of these T cells by staining with two anti-CD3ε Abs, one that is cross-reactive with human and NHP and a second that is only reactive against human CD3ε (Fig. 1E). We noted that nearly all the *Mamu* CD1b-GMM–specific T cells failed to stain with Abs targeting CD4 or CD8 coreceptors, which is in contrast to studies using *H. sapiens* CD1b-GMM that have revealed mostly $CD4^+$ T cells in humans (Fig. 1F) (58). Finally, we noted that T cells that were identified using *Mamu* CD1b-GMM tetramer largely fail to costain with *H. sapiens* CD1b-GMM tetramer (Fig. 1G). Thus, GMM-specific T cells are present within the CD1b-restricted T cell repertoire of rhesus macaques but are largely "invisible" without a species-specific tetramer to identify them.

GMM is presented to mutually exclusive T cell populations by CD1b and CD1c in humans

Several studies have confirmed that GMM is presented to T cells by CD1b in humans (12, 17, 58, 59), so it was not surprising to find the same was true in rhesus macaques. However, a recent study examining rhesus macaques after repeated vaccination with BCG and liposomal GMM suggested that the dominant mechanism by which GMM is presented to T cells might be mediated by CD1c instead of CD1b (39). To investigate this possibility in humans, we incubated PBMC from a South African adolescent with latent tuberculosis infection with allogeneic dendritic cells that express all human CD1 isoforms and C_{32}-GMM, allowing for selective expansion of Ag-specific T cells. Two weeks later, we noted that 0.4% of T cells stained with *H. sapiens* CD1b–C_{32}-GMM tetramer but not with mock-loaded CD1b control tetramer (Fig. 2A). We also observed 0.1% of T cells stained with *H. sapiens* CD1c–C_{32}-GMM tetramer but not with mock-loaded CD1c (Fig. 2A). These cells were independently sorted and successfully expanded ∼100-fold into T cell lines (Fig. 2B). The CD1c-GMM–restricted T cell line (cG11) stained only with CD1c-GMM tetramer and not with CD1c mock-loaded or CD1b-GMM tetramer (Fig. 2B, 2C). The CD1b-GMM–restricted T cell line (bG11) stained only with CD1b-GMM tetramer and not with CD1b mock-loaded or CD1c-GMM tetramer (Fig. 2B, 2C). Both bG11 and cG11 also largely failed to stain with CD1b and CD1c tetramers loaded with irrelevant mycobacterial lipid Ags (Ac_2SGL and PM, respectively) (Fig. 2D) (18, 20). We used K652 cells stably transfected with

Table I. Summary of tests of molecular evolution across primates in CD1a, CD1b, and CD1c paralogs

CD1 Paralog	M8A (Neutral Model)	M8 (Positive Selection)	2ΔlogL	*p* Value
CD1A	$p_0 = 0.4533$, $p = 0.0050$, $q = 67.7584$ $p_1 = 0.6147$, $\omega = 1.0000$	$p_0 = 0.8848$, $p = 0.0245$, $q = 0.0209$ $p_1 = 0.1152$, $\omega = 4.800$	58.4007	1.1×10^{-14}
CD1B	$p_0 = 0.5473$, $p = 0.0050$, $q = 40.4342$ $p_1 = 0.4527$, $\omega = 1.0000$	$p_0 = 0.6643$, $p = 0.0050$, $q = 2.6196$ $p_1 = 0.3357$, $\omega = 1.6799$	3.2376	0.036
CD1C	$p_0 = 0.4416$, $p = 0.0050$, $q = 10.9279$ $p_1 = 0.5584$, $\omega = 1.0000$	$p_0 = 0.7108$, $p = 21.0482$, $q = 99.0000$ $p_1 = 0.2892$, $\omega = 2.6905$	16.4367	2.5×10^{-5}

For each paralog, sequences were aligned using Clustal Ω, and tests of positive selection were performed using the codeml application in PAML (v4.8) with the primate species tree. Nested models of neutral evolution (M8a) and one allowing for positive selection (M8) were compared. In both models, the fraction of sites under purifying selection (p_0) are described by evolutionary rates (nonsynonymous to synonymous substitution rates, or d_N/d_S) drawn from a β distribution with parameters p and q. Under the neutral M8a model, the remaining sites ($p_1 = 1 - p_0$) are described by an additional dN/dS term (ω) constrained to 1. Under the positive-selection M8 model, ω is a free parameter that can be >1. The two models were compared by likelihood-ratio test with 1 df, and if significant, sites with Bayes-empirical Bayes-posterior probabilities ≥0.8 were considered under positive selection. CD1A and CD1C show stronger evidence of positive selection compared with CD1B during primate evolution.

single isoforms of *H. sapiens* CD1 proteins to further investigate the specificity of bG11 and cG11 T cell lines. Using IFN-γ ELISPOT, we found that bG11 was only activated in the presence of CD1b and GMM, whereas cG11 was only activated in the presence of CD1c and GMM (Fig. 2E, 2F). Together, these data reveal that C_{32}-GMM is recognized by two mutually exclusive T cell populations in humans, one that is restricted by CD1b and one that is restricted by CD1c.

Among CD1b-GMM–specific T cells within the bG11 T cell line, we noted that 8% expressed TRAV1-2, and 0.4% expressed TRBV4-1, whereas 2.5% expressed both TCR genes (Fig. 2G). Among CD1c-GMM–specific T cells within the cG11 T cell line, we noted that 99.9% stained with TRBV4-1 and found almost no evidence of TRAV1-2 expression (Fig. 2G). These data suggest that TRBV4-1 may be more important than TRAV1-2 for CD1c-mediated recognition of GMM (24, 25). The volume of the

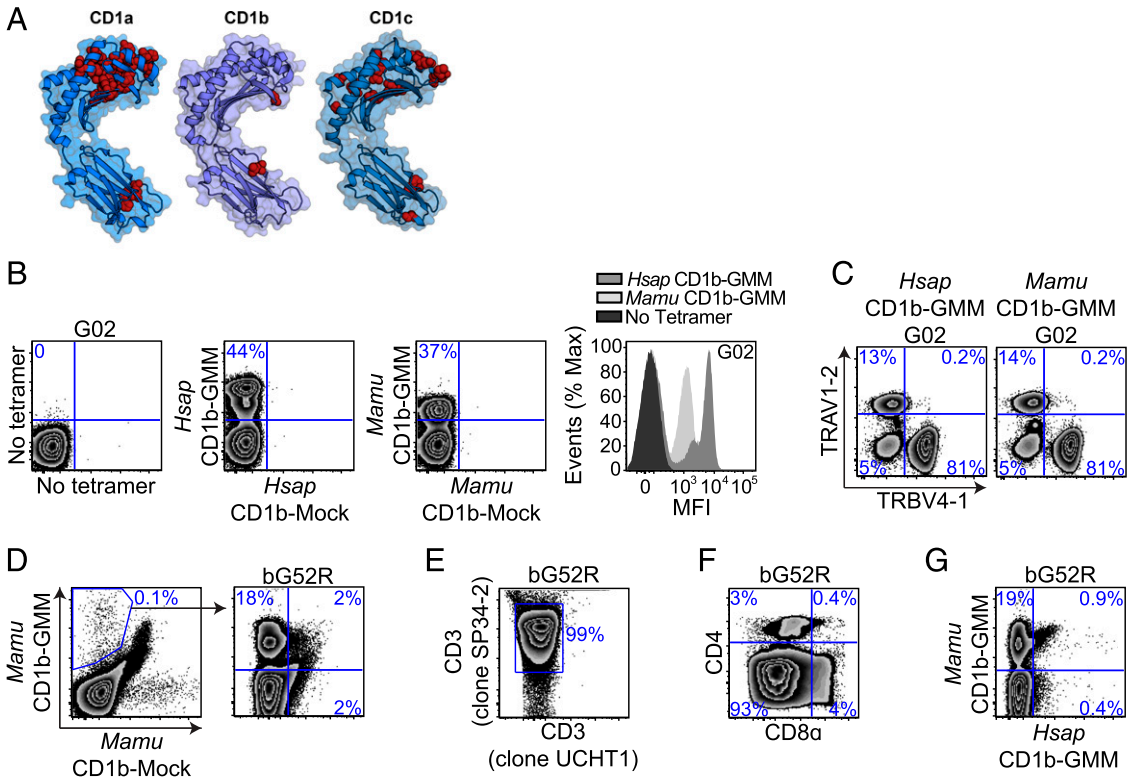

FIGURE 1. GMM is presented by CD1b to T cells in macaques. (**A**) Evolutionary genetics of group 1 CD1 genes among primates. CD1a, CD1b, and CD1c sequences were collated, aligned, and compared as described in the *Materials and Methods*. Amino acid residues under positive selection were modeled onto *H. sapiens* CD1 crystal structures using PyMOL v2.4 and are noted in red. (Protein Data Bank numbers 5J1A, 5L2J, and 3OV6 for CD1a, CD1b, and CD1c, respectively). (**B**) *H. sapiens* CD1b-GMM and *Mamu* CD1b-GMM tetramers were used to identify GMM-specific T cells present within a human T cell line (G02) by staining with both GMM-loaded (BV421) and mock-loaded (FITC) CD1b tetramers. Mean fluorescence intensities (MFI) of populations identified by *H. sapiens* and *Mamu* CD1b tetramers are compared using overlapping histograms. (**C**) GMM-specific T cells present within G02 were identified by staining with either *H. sapiens* CD1b-GMM or *Mamu* CD1b-GMM tetramers, and TCR genes expressed by GMM-specific T cells were identified using Abs targeting TRAV1-2 and TRBV4-1. (**D**) PBMC from an Indian-origin rhesus macaque that was vaccinated intradermally with BCG were stained with *Mamu* CD1b-GMM and *Mamu* CD1b mock-loaded tetramers, sorted, and expanded in vitro as described in the *Materials and Methods*. The resulting T cell line (bG52R) was restained with *Mamu* CD1b-GMM and *Mamu* CD1b mock-loaded tetramer. (**E**) The species origin of bG52R was confirmed by staining with an anti-CD3ε Ab (clone UCHT1) that does not bind with *Mamu* CD3ε as well as an anti-CD3ε Ab (clone SP34-2) that binds CD3ε from both species. (**F**) T cells staining with *Mamu* CD1b-GMM tetramer present within bG52R were further examined for coreceptor expression using Abs targeting CD4 and CD8α. (**G**) bG52R was simultaneously stained with *Mamu* CD1b-GMM tetramer (BV421) and *H. sapiens* CD1b-GMM tetramer (allophycocyanin). Data are representative of at least two independent experiments. See also Supplemental Fig. 1 and Table I.

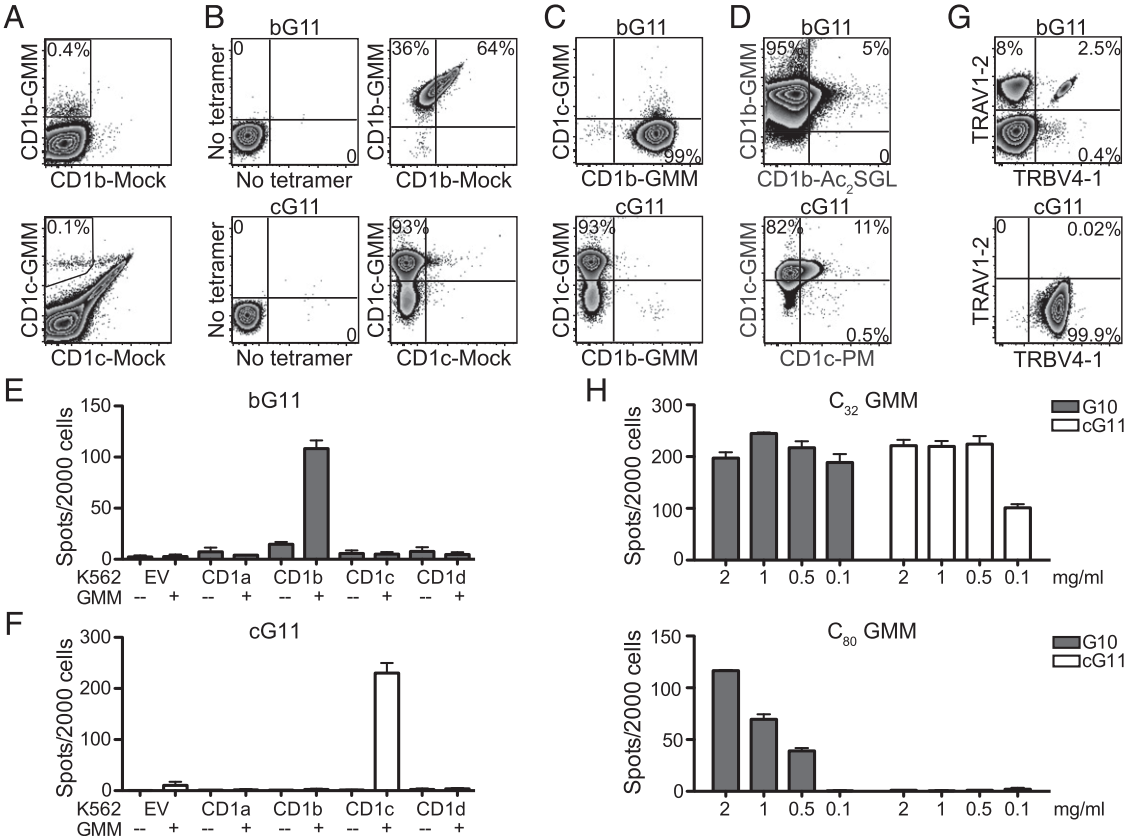

FIGURE 2. GMM is presented to mutually exclusive T cell populations by CD1b and CD1c in humans. (**A**) PBMC from a healthy South African adolescent were incubated with allogeneic dendritic cells, GMM, and IL-2 for 2 wk. The resulting T cell line was stained with either *H. sapiens* CD1b-GMM (allophycocyanin) and *H. sapiens* CD1b mock-loaded (PE) tetramers or *H. sapiens* CD1c-GMM (allophycocyanin) and *H. sapiens* CD1c mock-loaded (PE) tetramers to identify GMM-specific T cells. (**B**) T cells staining with *H. sapiens* CD1b-GMM tetramer were sorted and expanded in vitro to generate the bG11 T cell line. T cells stained with *H. sapiens* CD1c-GMM tetramer were sorted and expanded in vitro to generate the cG11 T cell line. (**C**) bG11 stains with *H. sapiens* CD1b-GMM tetramer (PE) but fails to costain with *H. sapiens* CD1c-GMM tetramer (allophycocyanin). cG11 stains with *H. sapiens* CD1c-GMM tetramer but fails to costain with *H. sapiens* CD1b-GMM tetramer. (**D**) bG11 stains specifically with *H. sapiens* CD1b-GMM tetramer (allophycocyanin) and fails to costain with *H. sapiens* CD1b (BV421) loaded with Ac_2SGL, another CD1b-presented mycobacterial lipid Ag. cG11 stains specifically with *H. sapiens* CD1c-GMM tetramer (PE) and fails to costain with *H. sapiens* CD1c (allophycocyanin) loaded with PM, another CD1c-presented mycobacterial lipid Ag. (**E**) bG11 or (**F**) cG11 were coincubated with K562 cells that were stably transfected with *H. sapiens* CD1a, CD1b, CD1c, CD1d, or EV, and IFN-γ production was measured by ELISPOT. (**G**) T cells within bG11 that stained with *H. sapiens* CD1b-GMM tetramer or T cells within cG11 that stained with *H. sapiens* CD1c-GMM tetramer were stained with Abs targeting TRAV1-2 and TRBV4-1 to investigate TCR gene usage. (**H**) A CD1b-GMM–restricted T cell line (G10) was coincubated with K562-CD1b–transfected APCs, and a CD1c-GMM–restricted T cell line (cG11) was coincubated with K562-CD1c–transfected APCs in the presence of titrating concentrations of short-chain (C_{32}) or long-chain (C_{80}) GMM. IFN-γ production was measured by ELISPOT. Data are representative of at least three (A–C and G) or two (D–F and H) independent experiments.

binding pocket of CD1b is nearly 50% larger than that of CD1c, so it is unclear whether the smaller CD1c cleft might accommodate C_{80}-GMM (60). We tested the ability of cG11 or a CD1b-restricted T cell line (G10) to recognize long-chain (C_{80}) or short-chain (C_{32}) GMM when presented by CD1-transfected K562 cells. The CD1b-restricted T cell line was able to recognize both C_{80}- and C_{32}-GMM in the presence of CD1b (Fig. 2H). However, cG11 was only activated by C_{32}-GMM in the presence of CD1c (Fig. 2H). Because *M. tuberculosis* and *M. bovis* appear to predominantly express C_{80}-GMM, these data support parallel mechanisms of Ag processing and presentation that facilitate the discrimination of bacterial lipids with identical head groups but different chain lengths (13, 61).

GMM is presented by CD1c to T cells in macaques

Having established that GMM is presented to T cells by CD1b and CD1c in humans, we proceeded to investigate this paradigm in NHP. We generated *Mamu* CD1c–C_{32}-GMM tetramers and stained PBMC obtained from a rhesus macaque 4 wk after intradermal BCG vaccination. We noted that *Mamu* CD1c-GMM tetramer stained 0.02% of T cells compared with *Mamu* CD1c-mock tetramer (Fig. 3A). These T cells were sorted and successfully expanded ~100-fold into a T cell line (cG52R) (Fig. 3B). We verified the species origin of these T cells by staining with two anti-CD3ε Abs as before (Fig. 3C). Within cG52R, we noted the majority of T cells expressed CD4, in contrast to bG52R, which was predominantly $CD4^-CD8^-$ (Figs. 1F, 3D). Finally, we noted that T cells that were identified using *Mamu* CD1c-GMM tetramer largely failed to costain with *H. sapiens* CD1c-GMM tetramer, demonstrating species specificity of the T cell response (Fig. 3E). However, GMM-specific T cells within cG52R were partially activated by K562 cells transfected with *H. sapiens* CD1c in the presence of GMM, demonstrating some cross-reactivity using a functional assay (Fig. 3F). These data reveal that in rhesus macaques, as with humans, C_{32}-GMM is presented by both CD1b and CD1c to two mutually exclusive populations of T cells.

Resident memory MAIT and iNKT cells are present in macaque lungs after i.v. BCG

Taking advantage of the donor-unrestricted nature of T cells that recognize these nonpolymorphic Ag-presenting molecules, we next

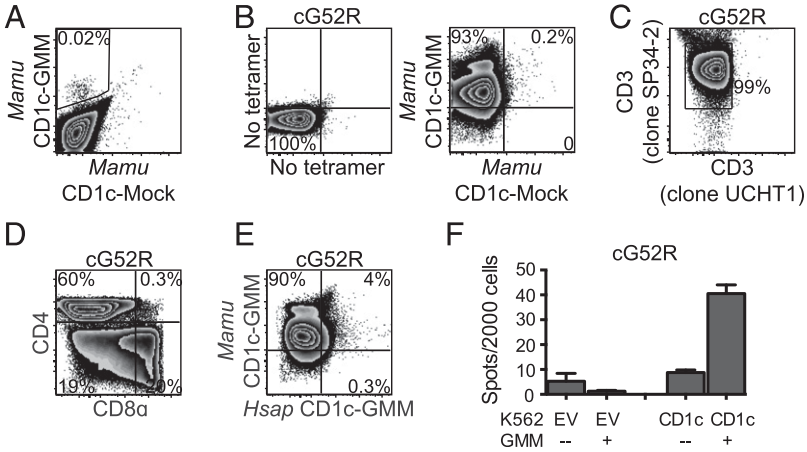

FIGURE 3. GMM is presented by CD1c to T cells in macaques. (**A**) PBMC from an Indian-origin rhesus macaque that was vaccinated intradermally with BCG were stained with *Mamu* CD1c-GMM (PE) and *Mamu* CD1c mock-loaded (BV421) tetramers to identify CD1c-GMM–specific T cells. (**B**) T cells staining with *Mamu* CD1c-GMM but not *Mamu* CD1c mock-loaded tetramer were sorted and expanded in vitro for 2 wk to generate a T cell line (cG52R). (**C**) The species origin of cG52R was confirmed by staining with an anti-CD3ε Ab (clone UCHT1) that does not bind *Mamu* CD3ε as well as an anti-CD3ε Ab (clone SP34-2) that binds CD3ε from both species. (**D**) T cells staining with *Mamu* CD1c-GMM tetramer present within cG52R were further examined for coreceptor expression using Abs targeting CD4 and CD8α. (**E**) cG52R was simultaneously stained with *Mamu* CD1c-GMM tetramer (G780) and *H. sapiens* CD1c-GMM tetramer (PE). Fewer than 5% of T cells staining with *Mamu* CD1c-GMM tetramer costain with *H. sapiens* CD1c-GMM tetramer. (**F**) cG52R was coincubated with K562-CD1c or K562-EV APCs in the presence or absence of GMM. IFN-γ detection by ELISPOT demonstrates the *Mamu*-derived T cell line is partially activated by *H. sapiens* CD1 proteins. Data are representative of at least three (A–E) or two (F) independent experiments.

sought to investigate whether mycobacterial vaccination might lead to the expansion of CD1- and MR1-restricted T cells and whether these T cells might be found among T cells resident in the lung (62, 63). To accomplish this, we made use of archived PBMC and BAL from our recent study, which demonstrated the superiority of i.v. BCG vaccination over standard routes in conferring protection from *M. tuberculosis* challenge (6). We developed a multiparameter flow cytometry panel to measure memory (CD45RA and CCR7), activation (HLA-DR and CD38), tissue-residency (CD69 and CD103), and T cell (CD4, CD8, and γδ) phenotypes of GMM-specific T cells with additional tetramers to profile mucosal-associated invariant T (MAIT) cells and iNKT cells. Our experiments were designed to answer two statistically independent questions: 1) are donor-unrestricted T cells induced in PBMC after i.v. BCG, and 2) is the distribution of donor-unrestricted T cells different between PBMC and BAL at the peak of the response to i.v. BCG?

Cryopreserved samples from 10 animals were chosen for analysis consisting of PBMC at baseline, PBMC at 4 wk postvaccination, and BAL at 4 wk postvaccination. When comparing 4 wk after i.v. BCG vaccination to baseline, we found no change in the frequency of MAIT cells ($p = 0.109$) (Supplemental Fig. 2A, 2B) nor in the frequency of iNKT cells ($p = 0.078$) (Supplemental Fig. 2C, 2D) in the blood. Although we did see that MAIT cells were found at higher frequency in the BAL compared with PBMC ($p = 0.008$) (Supplemental Fig. 2B), this did not hold true for iNKT cells ($p = 0.734$) (Supplemental Fig. 2D). These data are consistent with our published data, which revealed a selective induction of MAIT cells in BAL after i.v. BCG when compared with both aerosol and intradermal administration (6). We then used UMAP to examine whether subpopulations of MAIT or iNKT cells were expanded after i.v. BCG (Fig. 4A, 4F, Supplemental Fig. 3). Indeed, we observed an increase in the frequency of MAIT cells in PBMC expressing a $CD45RA^{-}CCR7^{-}$ T_{EM} phenotype ($p = 0.023$) (Fig. 4A–C). We also observed an increase in the frequency of MAIT cells expressing T_{RM} markers CD69 and CD103 in BAL compared with PBMC at the 4 wk time point ($p = 0.004$) (Fig. 4A, 4D, 4E). We observed similar expansions of iNKT cells expressing T_{EM} and T_{RM} markers in blood ($p = 0.078$) and BAL ($p = 0.008$), respectively (Fig. 4F–J). Notably, T cells with a T_{EM} phenotype were broadly expanded in the blood 4 wk after i.v. BCG ($p = 0.023$), and T cells expressing T_{RM} markers were broadly expanded in the BAL compared with the blood ($p = 0.004$) (Supplemental Fig. 2E, 2F). These data extend our published findings by revealing T_{RM} phenotypes in the lung as well as expansions of MAIT and iNKT cell subsets expressing T_{EM} phenotypes in the blood after i.v. BCG vaccination.

GMM-specific T cells are expanded after i.v. BCG

Finally, we examined the effect of i.v. BCG on CD1c-GMM–specific T cells (Fig. 5, Supplemental Fig. 3). Limiting cell numbers precluded us from simultaneously profiling CD1b-GMM–specific T cells in all samples. We prioritized the detection of CD1c-GMM–specific T cells based on the report by Morita et al. (39), which suggested that this was the dominant mechanism of GMM recognition by T cells in macaques. Specificity of staining and accurate quantification of low-frequency events were achieved by using two *Mamu* CD1c–C_{32}-GMM–loaded tetramers in different fluorescence channels as well as a mock-loaded negative-control CD1c tetramer (Fig. 5A, Supplemental Fig. 4). At baseline, we noted that the majority of *Mamu* CD1c-GMM–specific T cells expressed either a CD4 or CD8 coreceptor, which was consistent with our in vitro results (Figs. 3D, 5B). We observed an increase in the frequency of T cells staining with *Mamu* CD1c-GMM tetramers in PBMC at 4 wk after BCG vaccination compared with baseline ($p = 0.016$) (Fig. 5C). As with MAIT and iNKT cells, this expansion was especially pronounced within the T_{EM} subset ($p = 0.008$) (Fig. 5D–F). We noted a positive correlation between the frequency of CD1c-GMM–specific T cells and both iNKT ($r = 0.85$; $p = 0.002$) and MAIT cells ($r = 0.63$; $p = 0.051$) expressing a T_{EM} phenotype in the blood (Fig. 5G). By contrast, we observed a lower total frequency of T cells staining with *Mamu* CD1c-GMM tetramers in BAL compared with PBMC at the 4-wk time point ($p = 0.02$) (Fig. 5H). However, this was contrasted by a statistically significant difference in the subset of *Mamu* CD1c-GMM–specific T cells expressing T_{RM} markers

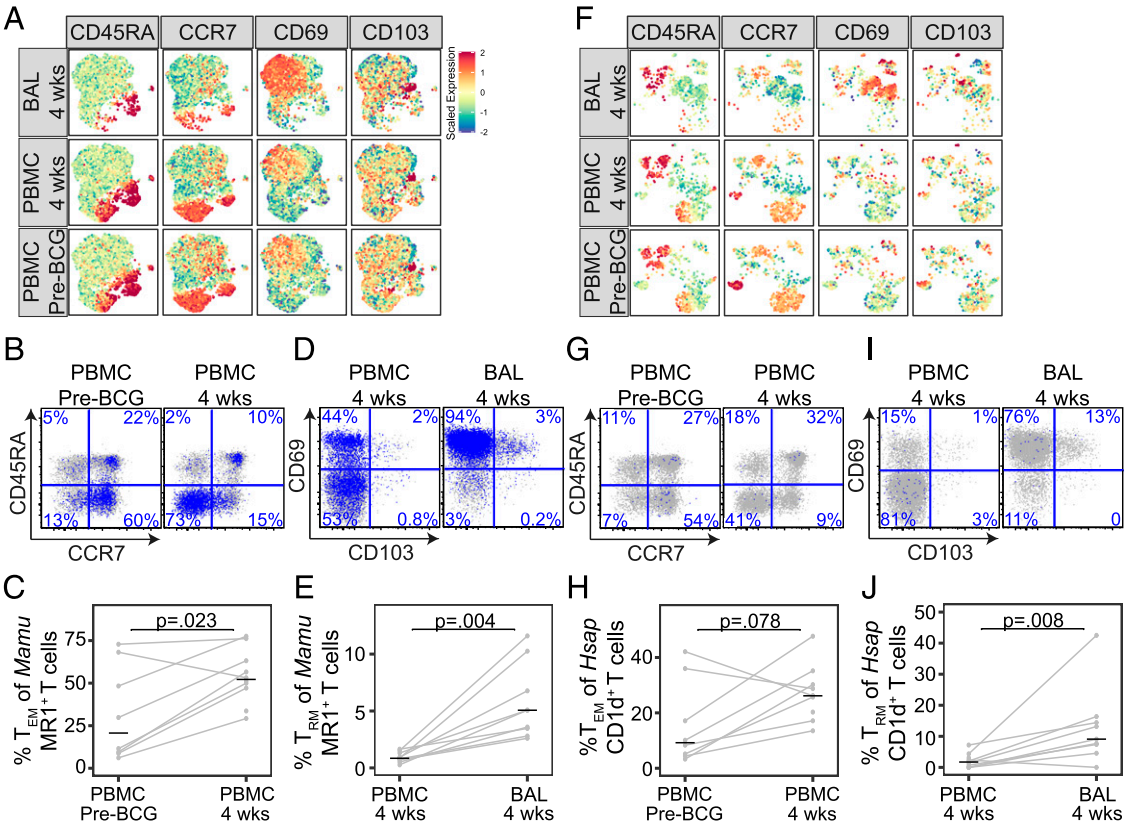

FIGURE 4. Resident memory MAIT and iNKT cells are present in macaque lungs after i.v. BCG. Multiparameter flow cytometry was used to profile T cells present in PBMC prior to i.v. BCG vaccination (pre-BCG) and in PBMC and BAL at 4 wk after BCG vaccination in 10 rhesus macaques. MAIT cells were identified using *Mamu* MR1–5-OP-RU loaded tetramer and iNKT cells were identified using *H. sapiens* CD1d–α-GalCer–loaded tetramer. (**A**) Expression of CD45RA, CCR7, CD69, and CD103 on MAIT cells is displayed after aggregating across all animals and performing dimensionality reduction with UMAP. Mean fluorescence intensities (MFI) were scaled to achieve a mean = 0 and SD = 1. (**B**) Representative staining of CD45RA and CCR7 among $CD8^+$ MAIT cells identified in PBMC from one animal pre-BCG or 4 wk after i.v. BCG vaccination. (**C**) The frequency of $CD4^+$ and $CD8^+$ MAIT cells expressing a T_{EM} phenotype was compared with pre-BCG and at 4 wk after i.v. BCG vaccination in all 10 animals. (**D**) Representative staining of CD69 and CD103 among $CD8^+$ MAIT cells identified in PBMC and BAL at 4 wk after i.v. BCG vaccination. (**E**) The frequency of $CD4^+$ and $CD8^+$ MAIT cells expressing a T_{RM} phenotype was compared in PBMC and BAL 4 wk after i.v. BCG vaccination in all 10 animals. (**F**) Expression of CD45RA, CCR7, CD69, and CD103 on iNKT cells is displayed after aggregating across all animals and performing dimensionality reduction with UMAP and scaling MFI as above. (**G**) Representative staining of CD45RA and CCR7 among $CD8^+$ iNKT cells identified in one animal pre-BCG or 4 wk after i.v. BCG vaccination. (**H**) The frequency of $CD4^+$ and $CD8^+$ iNKT cells expressing a T_{EM} phenotype was compared pre-BCG and at 4 wk after i.v. BCG vaccination. (**I**) Representative staining of CD69 and CD103 among $CD8^+$ iNKT cells identified in PBMC and BAL at 4 wk after i.v. BCG vaccination. (**J**) The frequency of $CD4^+$ and $CD8^+$ iNKT cells expressing a T_{RM} phenotype was compared pre-BCG and at 4 wk after i.v. BCG vaccination in all 10 animals. Results from line plots represent data from all animals. Statistical testing was performed using Wilcoxon signed-rank tests, and unadjusted *p* values are reported. The experiment was performed once. See also Supplemental Figs. 2 and 3.

($p = 0.008$) (Fig. 5D, 5I, 5J). These data reveal that i.v. BCG leads to clonal expansion and terminal differentiation of GMM-specific T cells in the blood. GMM-specific T cells are also detectable as T_{RM} cells in the lung.

Discussion

Our data advance several aspects of CD1 biology and tuberculosis vaccinology. First, we developed and validated *Mamu* CD1b-GMM and *Mamu* CD1c-GMM tetramers, establishing the NHP as a natural animal model in which to study the phenotypes and functions of CD1-reactive T cells in health and disease. Second, we discovered that both CD1b and CD1c can present GMM to T cells in humans and NHP, providing a potential mechanism for how primates evolved the capacity to discriminate among Ags with identical head groups but various lipid chain lengths. Third, we discovered that i.v. BCG leads to the expansion of GMM-specific T cells in the blood, which are also detectable in BAL fluid, suggesting that lipid Ag-specific T cells may contribute to the protective immune response to *M. tuberculosis*.

We specifically chose to study GMM-specific T cells in the setting of i.v. BCG vaccination because this route has been shown to provide superior protection compared with intradermal or aerosol vaccination in rhesus macaques, which are exquisitely susceptible to *M. tuberculosis* infection and disease (6, 7, 64). In our prior work, most animals vaccinated with i.v. BCG showed evidence of sterilizing immunity and had substantial expansions of MAIT cells in the lung at the time of *M. tuberculosis* challenge (6). The natural question is whether particular Ags are being targeted by lung T cells. Much effort is sure to be spent on distinguishing among the ~4000 proteins expressed by *M. tuberculosis*. Our data suggest that T cells mediating protective immunity may also be targeting lipids that are shared between BCG and *M. tuberculosis*, such as MA and GMM (65).

Morita et al. (39) were the first to describe the presentation of GMM by CD1c rather than CD1b in rhesus macaques by using an unusual vaccination strategy. GMM was purified from cultured mycobacteria and CD1c dependence was demonstrated through the use of blocking Abs and transfected APCs. Our data confirm

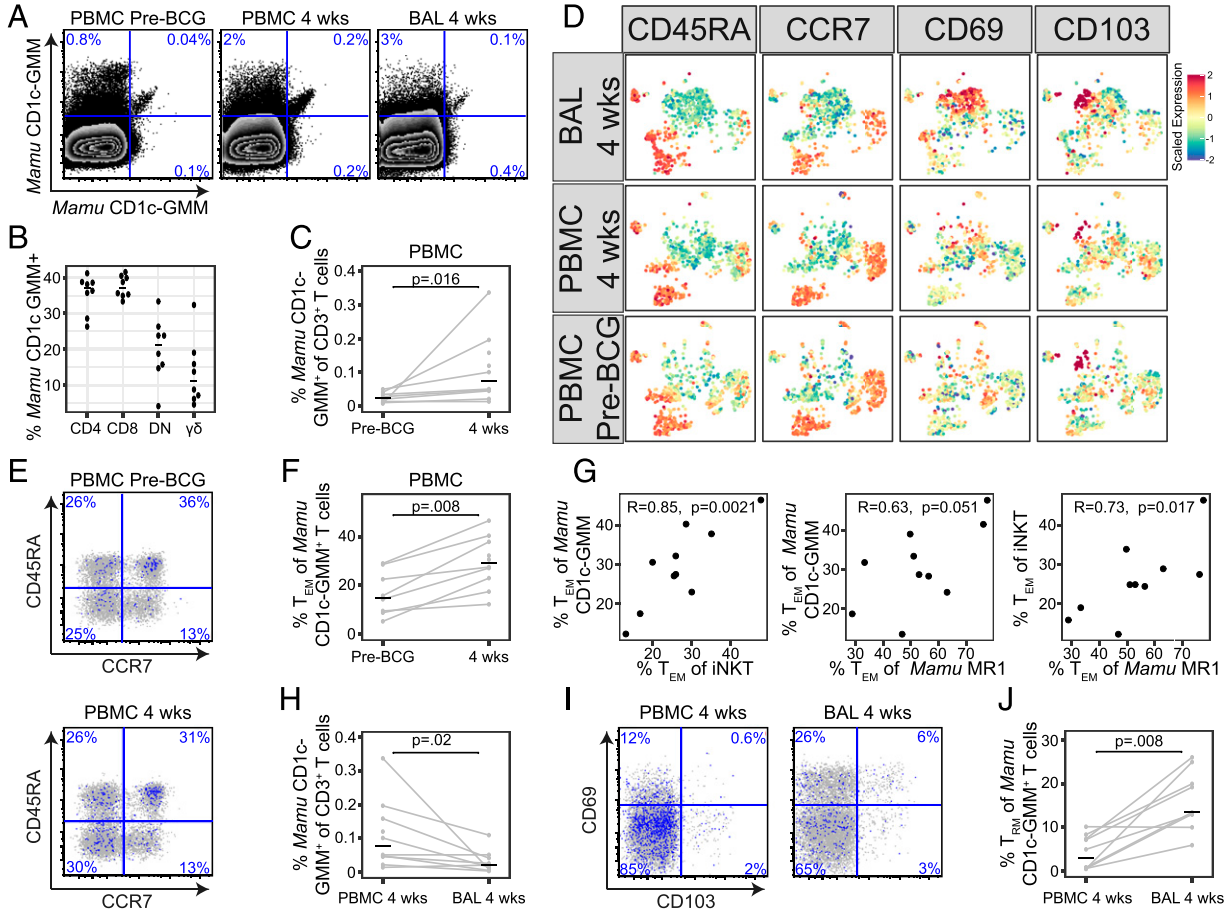

FIGURE 5. GMM-specific T cells are expanded after i.v. BCG. Multiparameter flow cytometry was used to profile GMM-specific T cells present in PBMC prior to i.v. BCG vaccination (pre-BCG) and in PBMC and BAL at 4 wk after BCG vaccination in rhesus macaques. (**A**) *Mamu* CD1c-GMM tetramers conjugated to (PE-Cy7) and (BV650) as well as mock-loaded *Mamu* CD1c (PerCP Cy5.5) were used to accurately identify GMM-specific T cells in PBMC or BAL. In one representative animal, there is an apparent increase in the frequency of T cells staining with both GMM-loaded tetramers at 4 wk after i.v. BCG. (**B**) CD4, CD8, and TCR-γδ expression among *Mamu* CD1c-GMM–specific T cells aggregated from all animals and analyzed directly ex vivo. (**C**) Frequencies of T cells staining with *Mamu* CD1c-GMM tetramer as a percentage of total $CD3^+$ cells in PBMC were compared between pre-BCG and 4 wk after i.v. BCG. (**D**) Expression of CD45RA, CCR7, CD69, and CD103 on T cells staining with *Mamu* CD1c-GMM tetramer is displayed after aggregating across all animals and performing dimensionality reduction with UMAP. Mean fluorescence intensities (MFI) were scaled to achieve a mean = 0 and SD = 1. (**E**) Representative staining of CD45RA and CCR7 among T cells staining with *Mamu* CD1c-GMM tetramer in one animal pre-BCG or 4 wk after i.v. BCG vaccination. (**F**) The frequency of *Mamu* CD1c-GMM staining T cells expressing a T_{EM} phenotype was compared pre-BCG and at 4 wk after i.v. BCG vaccination in all animals. (**G**) The frequency of cells expressing a T_{EM} phenotype as a percentage of total tetramer staining cells in the blood is plotted for CD1c-GMM versus iNKT cells, CD1c-GMM versus MAIT cells, or iNKT versus MAIT cells. Pearson correlation R and nominal *p* values are displayed for each comparison. (**H**) Frequencies of T cells staining with *Mamu* CD1c-GMM tetramer as a percentage of total $CD3^+$ cells were compared between PBMC and BAL at 4 wk after i.v. BCG vaccination. (**I**) Representative staining of CD69 and CD103 among T cells staining with *Mamu* CD1c-GMM tetramer in PBMC and BAL at 4 wk after i.v. BCG vaccination. (**J**) The frequency of T cells staining with *Mamu* CD1c-GMM tetramer expressing a T_{RM} phenotype was compared between PBMC and BAL at 4 wk after i.v. BCG vaccination. Statistical testing was performed using Wilcoxon signed-rank tests, and unadjusted *p* values are reported. The experiment was performed once. See also Supplemental Figs. 3 and 4.

and extend these findings through the use of synthetic GMM, newly validated *Mamu* CD1 tetramers, paired comparisons between blood and BAL, and context within i.v. BCG, which has been shown to protect against *M. tuberculosis* challenge. Importantly, we also show that CD1c is not capable of directly binding and presenting C_{80}-GMM, which is the dominant form of the lipid present in *M. tuberculosis* and likely BCG (61). C_{32}-GMM is ubiquitous among nontuberculous mycobacteria and related bacteria, so NHP may have first primed a T cell response to GMM through environmental exposure (22). Subsequent vaccination with intradermal or i.v. BCG may have led to expansions of C_{32}-GMM–specific T cells through nonspecific inflammatory effects, as has been shown for MAIT cells (66). It is also possible that C_{80}-GMM undergoes intracellular processing prior to loading onto CD1c. This would be in contrast to CD1b, which efficiently loads C_{80}-GMM through the endosome in dendritic cells (22). Thus, both our work and that of Morita et al. (39) highlight the fact that BCG vaccination induces a GMM-specific T cell response in NHP that may be Ag dependent or Ag independent.

Lung-resident memory CD4 T cells are induced by BCG in mice and associated with protection against *M. tuberculosis* challenge (67, 68). Notably, the frequency of T_{RM} is greater with the mucosal compared with the intradermal route (69). We have also noted that induction of lung parenchymal T cells is greater with i.v. compared with intradermal or aerosol routes of BCG vaccination in macaques (6). In this study, we defined GMM-specific T cells as T_{RM} in BAL by virtue of costaining with canonical markers CD69 and CD103. Because baseline BAL samples were unavailable, we cannot conclude that these cells were induced by i.v. BCG. At a minimum, our data show GMM-specific T cells are

detectable in the lungs 4 wk after i.v. BCG and express an activated phenotype. Because we have previously reported that residual BCG is detectable in BAL at this time point, it is possible that some of these cells may also represent activated T cells because of the persistence of mycobacterial Ag (6). Whether they persist as true resident memory T cells, express antibacterial functions, and contribute directly to reducing bacterial burdens in the lung is the subject of future work.

When we used *H. sapiens* CD1b-GMM and *H. sapiens* CD1c-GMM tetramer to isolate GMM-specific T cell lines, we found that they stained only with the tetramer used to isolate them. These data suggest that the TCR repertoires identified by these tetramers are mutually exclusive. CD1b-restricted T cells specific for GMM can express TRAV1-2 or TRBV4-1 as well as diverse TCRs (57, 70). CD1c-autoreactive T cells have been shown to preferentially express TRBV4-1 (25). A detailed molecular study of both GMM-specific and autoreactive CD1b-restricted T cells showed that germline-encoded residues within TRBV4-1 are essential for binding both CD1b and CD1c independent of the ligand (24). We find that nearly all T cells that stain with *H. sapiens* CD1c-GMM tetramer express TRAV4-1, but only a subset of T cells identified by *H. sapiens* CD1b-GMM express either TRAV1-2 or TRBV4-1. This is consistent with a diverse repertoire among *H. sapiens* CD1b-GMM T cells that may not hold for *H. sapiens* CD1c (70).

Validation of *Mamu* CD1b and CD1c tetramers and the discovery of tissue phenotypes of CD1c-GMM–specific T cells in rhesus macaques represents direct evidence for tissue-specific, polyclonal responses to CD1-presented lipid Ags. Studies in humans have advanced our understanding of the structure, function, and regulation of CD1 expression (60, 71). Access to peripheral blood and tissues have enabled the study of T cell phenotypes using tetramers and sequencing (15, 26). However, a deeper understanding of the role that CD1a-, CD1b-, and CD1c-restricted T cells play in disease pathogenesis has been stymied because of a lack of a suitable animal. The hCD1Tg mouse has partially solved that problem but is limited by the fact that the mouse is not a natural host for *M. tuberculosis*. There have also been attempts to leverage the cow or guinea pig for these studies but with limited success (72, 73). *Mamu* CD1b and CD1c tetramers loaded with specific ligands can now be used to interrogate the immune response in blood or at the site of infection in NHP, which phenocopy many aspects of human tuberculosis (74).

Acknowledgments

We acknowledge Dr. Branch Moody (Brigham & Women's Hospital) for providing K562-CD1–transfected APCs and purified C_{32}-GMM as well as critical review of the manuscript, and we thank the Washington National Primate Research Center for blood and tissue samples that facilitated pilot experiments.

Disclosures

The authors have no financial conflicts of interest.

References

1. Dockrell, H. M., and S. G. Smith. 2017. What have we learnt about BCG vaccination in the last 20 years? *Front. Immunol.* 8: 1134.
2. Colditz, G. A., C. S. Berkey, F. Mosteller, T. F. Brewer, M. E. Wilson, E. Burdick, and H. V. Fineberg. 1995. The efficacy of bacillus Calmette-Guérin vaccination of newborns and infants in the prevention of tuberculosis: meta-analyses of the published literature. *Pediatrics* 96: 29–35.
3. Colditz, G. A., T. F. Brewer, C. S. Berkey, M. E. Wilson, E. Burdick, H. V. Fineberg, and F. Mosteller. 1994. Efficacy of BCG vaccine in the prevention of tuberculosis. Meta-analysis of the published literature. *JAMA* 271: 698–702.
4. Flynn, J. L., M. M. Goldstein, K. J. Triebold, B. Koller, and B. R. Bloom. 1992. Major histocompatibility complex class I-restricted T cells are required for resistance to *Mycobacterium tuberculosis* infection. *Proc. Natl. Acad. Sci. USA* 89: 12013–12017.
5. Chen, C. Y., D. Huang, R. C. Wang, L. Shen, G. Zeng, S. Yao, Y. Shen, L. Halliday, J. Fortman, M. McAllister, et al. 2009. A critical role for CD8 T cells in a nonhuman primate model of tuberculosis. *PLoS Pathog.* 5: e1000392.
6. Darrah, P. A., J. J. Zeppa, P. Maiello, J. A. Hackney, M. H. Wadsworth, II, T. K. Hughes, S. Pokkali, P. A. Swanson, II, N. L. Grant, M. A. Rodgers, et al. 2020. Prevention of tuberculosis in macaques after intravenous BCG immunization. *Nature* 577: 95–102.
7. Sharpe, S., A. White, C. Sarfas, L. Sibley, F. Gleeson, A. McIntyre, R. Basaraba, S. Clark, G. Hall, E. Rayner, et al. 2016. Alternative BCG delivery strategies improve protection against *Mycobacterium tuberculosis* in non-human primates: protection associated with mycobacterial antigen-specific CD4 effector memory T-cell populations. *Tuberculosis (Edinb.)* 101: 174–190.
8. Zinkernagel, R. M., and P. C. Doherty. 1974. Restriction of in vitro T cell-mediated cytotoxicity in lymphocytic choriomeningitis within a syngeneic or semiallogeneic system. *Nature* 248: 701–702.
9. Porcelli, S., C. T. Morita, and M. B. Brenner. 1992. CD1b restricts the response of human CD4-8- T lymphocytes to a microbial antigen. *Nature* 360: 593–597.
10. Van Rhijn, I., D. Ly, and D. B. Moody. 2013. CD1a, CD1b, and CD1c in immunity against mycobacteria. *Adv. Exp. Med. Biol.* 783: 181–197.
11. Beckman, E. M., S. A. Porcelli, C. T. Morita, S. M. Behar, S. T. Furlong, and M. B. Brenner. 1994. Recognition of a lipid antigen by CD1-restricted alpha beta+ T cells. *Nature* 372: 691–694.
12. Moody, D. B., B. B. Reinhold, M. R. Guy, E. M. Beckman, D. E. Frederique, S. T. Furlong, S. Ye, V. N. Reinhold, P. A. Sieling, R. L. Modlin, et al. 1997. Structural requirements for glycolipid antigen recognition by CD1b-restricted T cells. *Science* 278: 283–286.
13. Layre, E., A. Collmann, M. Bastian, S. Mariotti, J. Czaplicki, J. Prandi, L. Mori, S. Stenger, G. De Libero, G. Puzo, and M. Gilleron. 2009. Mycolic acids constitute a scaffold for mycobacterial lipid antigens stimulating CD1-restricted T cells. *Chem. Biol.* 16: 82–92.
14. Seshadri, C., L. Lin, T. J. Scriba, G. Peterson, D. Freidrich, N. Frahm, S. C. DeRosa, D. B. Moody, J. Prandi, M. Gilleron, et al. 2015. T cell responses against mycobacterial lipids and proteins are poorly correlated in South African adolescents. *J. Immunol.* 195: 4595–4603.
15. Layton, E. D., K. K. Q. Yu, M. T. Smith, T. J. Scriba, S. C. De Rosa, and C. Seshadri. 2018. Validation of a CD1b tetramer assay for studies of human mycobacterial infection or vaccination. *J. Immunol. Methods* 458: 44–52.
16. Gilleron, M., S. Stenger, Z. Mazorra, F. Wittke, S. Mariotti, G. Böhmer, J. Prandi, L. Mori, G. Puzo, and G. De Libero. 2004. Diacylated sulfoglycolipids are novel mycobacterial antigens stimulating CD1-restricted T cells during infection with *Mycobacterium tuberculosis. J. Exp. Med.* 199: 649–659.
17. Kasmar, A. G., I. van Rhijn, T.-Y. Cheng, M. Turner, C. Seshadri, A. Schiefner, R. C. Kalathur, J. W. Annand, A. de Jong, J. Shires, et al. 2011. CD1b tetramers bind αβ T cell receptors to identify a mycobacterial glycolipid-reactive T cell repertoire in humans. *J. Exp. Med.* 208: 1741–1747.
18. Ly, D., A. G. Kasmar, T.-Y. Cheng, A. de Jong, S. Huang, S. Roy, A. Bhatt, R. P. van Summeren, J. D. Altman, W. R. Jacobs, Jr, et al. 2013. CD1c tetramers detect ex vivo T cell responses to processed phosphomycoketide antigens. *J. Exp. Med.* 210: 729–741.
19. Kasmar, A. G., I. Van Rhijn, K. G. Magalhaes, D. C. Young, T.-Y. Cheng, M. T. Turner, A. Schiefner, R. C. Kalathur, I. A. Wilson, M. Bhati, et al. 2013. Cutting edge: CD1a tetramers and dextramers identify human lipopeptide-specific T cells ex vivo. *J. Immunol.* 191: 4499–4503.
20. James, C. A., K. K. Q. Yu, M. Gilleron, J. Prandi, V. R. Yedulla, Z. Z. Moleda, E. Diamanti, M. Khan, V. K. Aggarwal, J. F. Reijneveld, et al. 2018. CD1b tetramers identify T cells that recognize natural and synthetic diacylated sulfoglycolipids from *Mycobacterium tuberculosis. Cell Chem. Biol.* 25: 392–402.e14.
21. Van Rhijn, I., S. K. Iwany, P. Fodran, T. Y. Cheng, L. Gapin, A. J. Minnaard, and D. B. Moody. 2017. CD1b-mycolic acid tetramers demonstrate T-cell fine specificity for mycobacterial lipid tails. *Eur. J. Immunol.* 47: 1525–1534.
22. Moody, D. B., V. Briken, T. Y. Cheng, C. Roura-Mir, M. R. Guy, D. H. Geho, M. L. Tykocinski, G. S. Besra, and S. A. Porcelli. 2002. Lipid length controls antigen entry into endosomal and nonendosomal pathways for CD1b presentation. *Nat. Immunol.* 3: 435–442.
23. Gras, S., I. Van Rhijn, A. Shahine, T. Y. Cheng, M. Bhati, L. L. Tan, H. Halim, K. D. Tuttle, L. Gapin, J. Le Nours, et al. 2016. T cell receptor recognition of CD1b presenting a mycobacterial glycolipid. *Nat. Commun.* 7: 13257.
24. Reinink, P., A. Shahine, S. Gras, T.-Y. Cheng, R. Farquhar, K. Lopez, S. A. Suliman, J. F. Reijneveld, J. Le Nours, L. L. Tan, et al. 2019. A TCR β-chain motif biases toward recognition of human CD1 proteins. *J. Immunol.* 203: 3395–3406.
25. Guo, T., M. Y. Koo, Y. Kagoya, M. Anczurowski, C.-H. Wang, K. Saso, M. O. Butler, and N. Hirano. 2018. A subset of human autoreactive CD1c-restricted T cells preferentially expresses TRBV4-1$^+$ TCRs. *J. Immunol.* 200: 500–511.
26. Lopez, K., S. K. Iwany, S. Suliman, J. F. Reijneveld, T. A. Ocampo, J. Jimenez, R. Calderon, L. Lecca, M. B. Murray, D. B. Moody, and I. Van Rhijn. 2020. CD1b tetramers broadly detect T cells that correlate with mycobacterial exposure but not tuberculosis disease state. *Front. Immunol.* 11: 199.
27. Behar, S. M., C. C. Dascher, M. J. Grusby, C. R. Wang, and M. B. Brenner. 1999. Susceptibility of mice deficient in CD1D or TAP1 to infection with *Mycobacterium tuberculosis. J. Exp. Med.* 189: 1973–1980.

28. Sada-Ovalle, I., M. Sköld, T. Tian, G. S. Besra, and S. M. Behar. 2010. α-galactosylceramide as a therapeutic agent for pulmonary *Mycobacterium tuberculosis* infection. *Am. J. Respir. Crit. Care Med.* 182: 841–847.
29. Dascher, C. C., and M. B. Brenner. 2003. Evolutionary constraints on CD1 structure: insights from comparative genomic analysis. *Trends Immunol.* 24: 412–418.
30. Felio, K., H. Nguyen, C. C. Dascher, H.-J. Choi, S. Li, M. I. Zimmer, A. Colmone, D. B. Moody, M. B. Brenner, and C.-R. Wang. 2009. CD1-restricted adaptive immune responses to Mycobacteria in human group 1 CD1 transgenic mice. *J. Exp. Med.* 206: 2497–2509.
31. Zhao, J., S. Siddiqui, S. Shang, Y. Bian, S. Bagchi, Y. He, and C. R. Wang. 2015. Mycolic acid-specific T cells protect against *Mycobacterium tuberculosis* infection in a humanized transgenic mouse model. *Elife* 4: e08525.
32. Chancellor, A., A. S. Tocheva, C. Cave-Ayland, L. Tezera, A. White, J. R. Al Dulayymi, J. S. Bridgeman, I. Tews, S. Wilson, N. M. Lissin, et al. 2017. CD1b-restricted GEM T cell responses are modulated by *Mycobacterium tuberculosis* mycolic acid meromycolate chains. *Proc. Natl. Acad. Sci. USA* 114: E10956–E10964.
33. Ogongo, P., A. J. C. Steyn, F. Karim, K. J. Dullabh, I. Awala, R. Madansein, A. Leslie, and S. M. Behar. 2020. Differential skewing of donor-unrestricted and γδ T cell repertoires in tuberculosis-infected human lungs. *J. Clin. Invest.* 130: 214–230.
34. Reinink, P., and I. Van Rhijn. 2016. Mammalian CD1 and MR1 genes. *Immunogenetics* 68: 515–523.
35. Yu, K. K. Q., D. B. Wilburn, J. A. Hackney, P. A. Darrah, K. E. Foulds, C. A. James, M. T. Smith, L. Jing, R. A. Seder, M. Roederer, et al. 2019. Conservation of molecular and cellular phenotypes of invariant NKT cells between humans and non-human primates. *Immunogenetics* 71: 465–478.
36. Motsinger, A., A. Azimzadeh, A. K. Stanic, R. P. Johnson, L. Van Kaer, S. Joyce, and D. Unutmaz. 2003. Identification and simian immunodeficiency virus infection of CD1d-restricted macaque natural killer T cells. *J. Virol.* 77: 8153–8158.
37. Gansuvd, B., W. J. Hubbard, A. Hutchings, F. T. Thomas, J. Goodwin, S. B. Wilson, M. A. Exley, and J. M. Thomas. 2003. Phenotypic and functional characterization of long-term cultured rhesus macaque spleen-derived NKT cells. *J. Immunol.* 171: 2904–2911.
38. Morita, D., K. Katoh, T. Harada, Y. Nakagawa, I. Matsunaga, T. Miura, A. Adachi, T. Igarashi, and M. Sugita. 2008. Trans-species activation of human T cells by rhesus macaque CD1b molecules. *Biochem. Biophys. Res. Commun.* 377: 889–893.
39. Morita, D., Y. Hattori, T. Nakamura, T. Igarashi, H. Harashima, and M. Sugita. 2013. Major T cell response to a mycolyl glycolipid is mediated by CD1c molecules in rhesus macaques. *Infect. Immun.* 81: 311–316.
40. Young, J. M., and B. J. Trask. 2007. V2R gene families degenerated in primates, dog and cow, but expanded in opossum. *Trends Genet.* 23: 212–215.
41. Sievers, F., A. Wilm, D. Dineen, T. J. Gibson, K. Karplus, W. Li, R. Lopez, H. McWilliam, M. Remmert, J. Söding, et al. 2011. Fast, scalable generation of high-quality protein multiple sequence alignments using Clustal Omega. *Mol. Syst. Biol.* 7: 539.
42. Purvis, A. 1995. A composite estimate of primate phylogeny. *Philos. Trans. R. Soc. Lond. B Biol. Sci.* 348: 405–421.
43. Swanson, W. J., R. Nielsen, and Q. Yang. 2003. Pervasive adaptive evolution in mammalian fertilization proteins. *Mol. Biol. Evol.* 20: 18–20.
44. van Summeren, R. P., D. B. Moody, B. L. Feringa, and A. J. Minnaard. 2006. Total synthesis of enantiopure β-D-mannosyl phosphomycoketides from *Mycobacterium tuberculosis*. *J. Am. Chem. Soc.* 128: 4546–4547.
45. Tahiri, N., P. Fodran, D. Jayaraman, J. Buter, M. D. Witte, T. A. Ocampo, D. B. Moody, I. Van Rhijn, and A. J. Minnaard. 2020. Total synthesis of a mycolic acid from *Mycobacterium tuberculosis*. *Angew. Chem. Int. Ed. Engl.* 59: 7555–7560.
46. O'Doherty, U., R. Ignatius, N. Bhardwaj, and M. Pope. 1997. Generation of monocyte-derived dendritic cells from precursors in rhesus macaque blood. *J. Immunol. Methods* 207: 185–194.
47. Dolton, G., K. Tungatt, A. Lloyd, V. Bianchi, S. M. Theaker, A. Trimby, C. J. Holland, M. Donia, A. J. Godkin, D. K. Cole, et al. 2015. More tricks with tetramers: a practical guide to staining T cells with peptide-MHC multimers. *Immunology* 146: 11–22.
48. Riddell, S. R., K. S. Watanabe, J. M. Goodrich, C. R. Li, M. E. Agha, and P. D. Greenberg. 1992. Restoration of viral immunity in immunodeficient humans by the adoptive transfer of T cell clones. *Science* 257: 238–241.
49. Le Roy, C., N. Varin-Blank, F. Ajchenbaum-Cymbalista, and R. Letestu. 2009. Flow cytometry APC-tandem dyes are degraded through a cell-dependent mechanism. *Cytometry A* 75: 882–890.
50. de Jong, A., V. Peña-Cruz, T. Y. Cheng, R. A. Clark, I. Van Rhijn, and D. B. Moody. 2010. CD1a-autoreactive T cells are a normal component of the human αβ T cell repertoire. *Nat. Immunol.* 11: 1102–1109.
51. Mahomed, H., T. Hawkridge, S. Verver, L. Geiter, M. Hatherill, D. A. Abrahams, R. Ehrlich, W. A. Hanekom, and G. D. Hussey, SATVI Adolescent Study Team. 2011. Predictive factors for latent tuberculosis infection among adolescents in a high-burden area in South Africa. *Int. J. Tuberc. Lung Dis.* 15: 331–336.
52. Finak, G., J. Frelinger, W. Jiang, E. W. Newell, J. Ramey, M. M. Davis, S. A. Kalams, S. C. De Rosa, and R. Gottardo. 2014. OpenCyto: an open source infrastructure for scalable, robust, reproducible, and automated, end-to-end flow cytometry data analysis. *PLOS Comput. Biol.* 10: e1003806.
53. R Core Team. 2016. *R: A Language and Environment for Statistical Computing*. R Foundation for Statistical Computing, Vienna, Austria.
54. Kim, J. H., Y. Hu, T. Yongqing, J. Kim, V. A. Hughes, J. Le Nours, E. A. Marquez, A. W. Purcell, Q. Wan, M. Sugita, et al. 2016. CD1a on Langerhans cells controls inflammatory skin disease. *Nat. Immunol.* 17: 1159–1166.
55. van Bebber, I. P., R. M. Mollen, J. P. Koopman, and R. J. Goris. 1989. Decontamination of the gastrointestinal tract and prevention of multiple organ failure. An experimental study. *Prog. Clin. Biol. Res.* 308: 827–833.
56. Scharf, L., N. S. Li, A. J. Hawk, D. Garzón, T. Zhang, L. M. Fox, A. R. Kazen, S. Shah, E. J. Haddadian, J. E. Gumperz, et al. 2010. The 2.5 Å structure of CD1c in complex with a mycobacterial lipid reveals an open groove ideally suited for diverse antigen presentation. *Immunity* 33: 853–862.
57. Van Rhijn, I., N. A. Gherardin, A. Kasmar, W. de Jager, D. G. Pellicci, L. Kostenko, L. L. Tan, M. Bhati, S. Gras, D. I. Godfrey, et al. 2014. TCR bias and affinity define two compartments of the CD1b-glycolipid-specific T Cell repertoire. *J. Immunol.* 192: 4054–4060.
58. Van Rhijn, I., A. Kasmar, A. de Jong, S. Gras, M. Bhati, M. E. Doorenspleet, N. de Vries, D. I. Godfrey, J. D. Altman, W. de Jager, et al. 2013. A conserved human T cell population targets mycobacterial antigens presented by CD1b. *Nat. Immunol.* 14: 706–713.
59. Moody, D. B., M. R. Guy, E. Grant, T. Y. Cheng, M. B. Brenner, G. S. Besra, and S. A. Porcelli. 2000. CD1b-mediated T cell recognition of a glycolipid antigen generated from mycobacterial lipid and host carbohydrate during infection. *J. Exp. Med.* 192: 965–976.
60. Van Rhijn, I., D. I. Godfrey, J. Rossjohn, and D. B. Moody. 2015. Lipid and small-molecule display by CD1 and MR1. *Nat. Rev. Immunol.* 15: 643–654.
61. Layre, E., L. Sweet, S. Hong, C. A. Madigan, D. Desjardins, D. C. Young, T. Y. Cheng, J. W. Annand, K. Kim, I. C. Shamputa, et al. 2011. A comparative lipidomics platform for chemotaxonomic analysis of *Mycobacterium tuberculosis*. *Chem. Biol.* 18: 1537–1549.
62. Joosten, S. A., T. H. M. Ottenhoff, D. M. Lewinsohn, D. F. Hoft, D. B. Moody, and C. Seshadri, Collaboration for Tuberculosis Vaccine Discovery - Donor-Unrestricted T-cells Working Group, Bill and Melinda Gates Foundation. 2019. Harnessing donor unrestricted T-cells for new vaccines against tuberculosis. *Vaccine* 37: 3022–3030.
63. Van Rhijn, I., and D. B. Moody. 2015. Donor unrestricted T cells: a shared human T cell response. *J. Immunol.* 195: 1927–1932.
64. Maiello, P., R. M. DiFazio, A. M. Cadena, M. A. Rodgers, P. L. Lin, C. A. Scanga, and J. L. Flynn. 2018. Rhesus macaques are more susceptible to progressive tuberculosis than cynomolgus macaques: a quantitative comparison. *Infect. Immun.* 86: e00505–e00517.
65. Layre, E., H. J. Lee, D. C. Young, A. J. Martinot, J. Buter, A. J. Minnaard, J. W. Annand, S. M. Fortune, B. B. Snider, I. Matsunaga, et al. 2014. Molecular profiling of *Mycobacterium tuberculosis* identifies tuberculosinyl nucleoside products of the virulence-associated enzyme Rv3378c. *Proc. Natl. Acad. Sci. USA* 111: 2978–2983.
66. Suliman, S., M. Murphy, M. Musvosvi, A. Gela, E. W. Meermeier, H. Geldenhuys, C. Hopley, A. Toefy, N. Bilek, A. Veldsman, et al. 2019. MR1-independent activation of human mucosal-associated invariant T cells by mycobacteria. *J. Immunol.* 203: 2917–2927.
67. Laidlaw, B. J., N. Zhang, H. D. Marshall, M. M. Staron, T. Guan, Y. Hu, L. S. Cauley, J. Craft, and S. M. Kaech. 2014. CD4+ T cell help guides formation of CD103+ lung-resident memory CD8+ T cells during influenza viral infection. *Immunity* 41: 633–645.
68. Perdomo, C., U. Zedler, A. A. Kühl, L. Lozza, P. Saikali, L. E. Sander, A. Vogelzang, S. H. E. Kaufmann, and A. Kupz. 2016. Mucosal BCG vaccination induces protective lung-resident memory T cell populations against tuberculosis. *mBio* 7: e01686-16.
69. Bull, N. C., E. Stylianou, D. A. Kaveh, N. Pinpathomrat, J. Pasricha, R. Harrington-Kandt, M. C. Garcia-Pelayo, P. J. Hogarth, and H. McShane. 2019. Enhanced protection conferred by mucosal BCG vaccination associates with presence of antigen-specific lung tissue-resident PD-1^{+} KLRG1^{-} CD4^{+} T cells. *Mucosal Immunol.* 12: 555–564.
70. DeWitt, W. S., K. K. Q. Yu, D. B. Wilburn, A. Sherwood, M. Vignali, C. L. Day, T. J. Scriba, H. S. Robins, W. J. Swanson, R. O. Emerson, et al. 2018. A diverse lipid antigen-specific TCR repertoire is clonally expanded during active tuberculosis. *J. Immunol.* 201: 888–896.
71. Moody, D. B., and R. N. Cotton. 2017. Four pathways of CD1 antigen presentation to T cells. *Curr. Opin. Immunol.* 46: 127–133.
72. Hiromatsu, K., C. C. Dascher, K. P. LeClair, M. Sugita, S. T. Furlong, M. B. Brenner, and S. A. Porcelli. 2002. Induction of CD1-restricted immune responses in guinea pigs by immunization with mycobacterial lipid antigens. *J. Immunol.* 169: 330–339.
73. Van Rhijn, I., A. P. Koets, J. S. Im, D. Piebes, F. Reddington, G. S. Besra, S. A. Porcelli, W. van Eden, and V. P. M. G. Rutten. 2006. The bovine CD1 family contains group 1 CD1 proteins, but no functional CD1d. *J. Immunol.* 176: 4888–4893.
74. Flynn, J. L., H. P. Gideon, J. T. Mattila, and P. L. Lin. 2015. Immunology studies in non-human primate models of tuberculosis. *Immunol. Rev.* 264: 60–73.